THE JOURNAL OF PHYSICAL CHEMISTRY LETTERS
A JOURNAL OF THE AMERICAN CHEMICAL SOCIETY

pubs.acs.org/JPCL Letter

Unveiling the Role of Spin Currents on the Giant Rashba Splitting in Single-Layer WSe_2

Alberto Boccuni, Bárbara Maria Teixeira Costa Peluzo, Filippo Bodo, Giacomo Ambrogio, Jefferson Maul, Davide Mitoli, Giovanni Vignale, Stefano Pittalis, Elfi Kraka, Jacques K. Desmarais,* and Alessandro Erba*

Cite This: *J. Phys. Chem. Lett.* 2024, 15, 7442−7448 Read Online

ACCESS | Metrics & More | Article Recommendations

ABSTRACT: The Rashba spin splitting in uniaxial, inversion-asymmetric materials has attracted considerable interest for spintronic applications. The most widely used theoretical framework to model such states is Kohn−Sham density functional theory (DFT) in combination with standard (semi)local exchange−correlation density functional approximations (DFAs). However, in the presence of spin−orbit coupling, DFT misses contributions due to modification of the many-body interaction by spin currents $\vec{\mathbf{J}}$. Inclusion of the latter effects requires a spin current DFT (SCDFT) formulation, which is seldom considered. We investigate the giant Rashba splitting in single-layer WSe_2, and we quantify the effect of including spin currents in DFAs of the SCDFT. Crucially, we show that SCDFT allows fully capturing the giant Rashba band splitting in single-layer WSe_2, otherwise previously systematically underestimated by standard (semi)local DFAs within the DFT framework. We find the inclusion of $\vec{\mathbf{J}}$ on the DFA increases the Rashba splitting by about 20%.

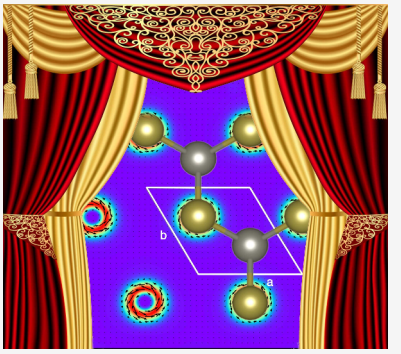

Transition-metal dichalcogenides (TMD) are layered materials of MX_2 stoichiometry (with X = S, Se, Te) that have attracted considerable interest in recent years. Depending on the metal (usually M = Mo, W), TMDs can be semiconductors, semimetals, or superconductors.[1−4] The electronic properties of TMDs can be effectively tuned by controlling their thickness.[5−10] In particular, single-layer TMDs, because of various quantum confinement effects, combine peculiar electronic, optical, and mechanical properties, which make them promising for flexible electronics and optoelectronics.[11−16] For instance, because of their semiconducting band gap of about 1.1−2.0 eV,[17,18] TMD single layers are considered good candidates as channel materials in field-effect transistors (FETs) and solar cells.[19−21] In particular, single-layer TMDs allow for a more efficient gate tunability and for a larger current on−off ratio than their multilayer counterparts.[19] The band gap is likely of direct $K \rightarrow K$ nature, with a quasi-degenerate indirect $K \rightarrow Q$ transition, which can be stabilized by strain engineering.[22−28]

Space inversion symmetry (SIS) breaking and time-reversal symmetry (TRS) preservation, together with large spin−orbit coupling (SOC), induce giant Rashba type I spin splitting at the top of the valence band (VB) in single-layer TMDs of about 150−500 meV at K.[29,30] Additionally, the interplay between inversion asymmetry and SOC yields a smaller spin splitting between the two lowest lying conduction bands (CB) in the K valley,[31] which was very recently measured at about 12 meV for both WS_2 and WSe_2 single layers by photoluminescence.[32]

Theoretical calculations based on the density functional theory (DFT)—with a description of the spin−orbit interaction—have played a crucial role in the investigation of the exotic physics of this class of 2D materials.[22,29,33−39] Indeed, most electronic structure packages can deal with SOC by inclusion of the corresponding one-body term in the Kohn−Sham (KS) equations and treat it either self-consistently or through second-variational approaches.[40−45] But the DFT Hamiltonian does not include SOC! Thus, formally, DFT—which adopts energy functionals of the form $E_{xc}[n]$ with n being the particle-number density—can not deal with SOC nonperturbatively. An inclusion of SOC in the Hamiltonian leads directly to the spin-current DFT (SCDFT), involving energy functionals $E_{xc}[n, \vec{\mathbf{J}}]$ depending also on the *noncollinear* spin-currents $\mathbf{J}^x$, $\mathbf{J}^y$, and $\mathbf{J}^z$.[46,47] Also note that $\mathbf{J}$, being the tensor product of spin and ordinary current, is a time-reversal invariant quantity.[48,49] Applications of SCDFT to real materials thus require extensions of regular density

Received: May 30, 2024
Revised: July 10, 2024
Accepted: July 10, 2024

https://doi.org/10.1021/acs.jpclett.4c01607
J. Phys. Chem. Lett. 2024, 15, 7442−7448

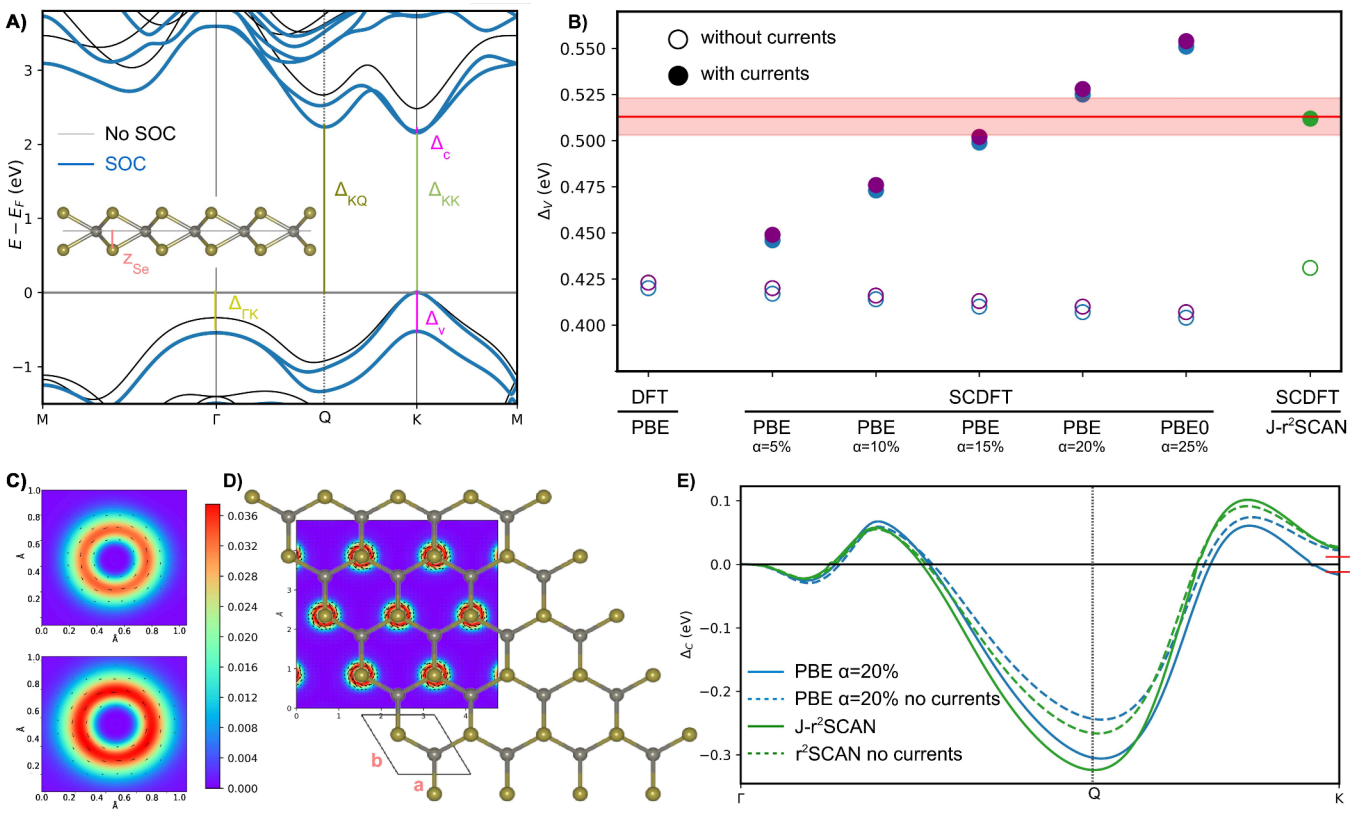

Figure 1. (A) Electronic band structure of 2D single-layer WSe_2 with (blue line) and without (black line) SOC. The main band splittings and transitions are highlighted. (B) Valence Rashba splitting Δ_v according to DFT and different versions of SCDFT. Empty and full symbols correspond to calculations without and with a dependence on the spin current density $\vec{\mathbf{J}}$ of the xc potential, respectively. For PBE-based calculations, results are also shown from geometry optimizations with SOC (purple versus blue symbols). The horizontal red line and area mark the experimental value along with its uncertainty: 513 ± 10 meV. (C) Color maps of the spatial distribution of $\boldsymbol{J}^z$ in the *xy* plane close to a Se atom computed without (top) and with (bottom) inclusion of the spin current density in the xc potential. The color identifies the absolute value of the reported quantity, while the length and direction of the superimposed black arrows represent the magnitude and direction of their in-plane Cartesian components. (D) Top view of the atomic structure of single-layer WSe_2, superimposed to a color map of the distribution of $\boldsymbol{J}^z$, in the *xy* plane of the Se atoms, highlighting its spatial localization close to the atomic centers. (E) Conduction Rashba splitting Δ_c along the Γ−*K* path as computed without (dashed lines) and with (solid lines) inclusion of the spin current density in the xc potential; red segments mark the experimental value at *K* of 12 ± 0.5 meV. Data in panels A, C, and D are computed with the PBE xc functional with a fraction of Fock exchange α = 20%. Spin current density maps and band plots are produced with the CRYSTALpytools Python interface to CRYSTAL.[72]

functional approximations (DFAs) as well as extended self-consistent field procedures.

In setting up a SCDFT-based approach, it is crucial to take into account that $\vec{\mathbf{J}}$ is not a U(1) × SU(2) gauge-invariant quantity, while the xc energy itself is—and thus approximations thereof must be—gauge-invariant. As a result, only certain combinations of densities may legitimately appear in E_{xc}, which typically require explicitly orbital-dependent functionals.[50−52] For instance, one solution is provided within the domain of meta-generalized-gradient approximations (MGGAs) from the fact that, for the time-reversal invariant states here considered, the combination $\tau - \mathbf{J}^a \cdot \mathbf{J}^a/2n$ is gauge-invariant (here $\tau = \frac{1}{2}\sum_k \Phi_k^\dagger \Phi_k$ is the explicitly orbital-dependent kinetic energy-density, and Φ_k are the Generalized Kohn−Sham orbitals).[50,52,53] Alternatively, nonlocal Fock exchange (and thus hybrid DFAs) offer a straightforward way of capturing SOC self-consistently without invoking spin currents explicitly.[52] At small interparticle separation, a one-to-one correspondence may be established between spin-blocks of the complex density matrix (and thus of the Fock potential) and spin currents.[52] To keep the discussion compact, in the following we shall say that currents are included or not included in hybrid calculations, when corresponding spin-blocks of the Fock potential are included or not included, as explained in ref 54.

In this Letter, we analyze SOC-induced modifications to the electronic band structure of single-layer WSe_2 (including band gaps and Rashba band splittings in the top of the valence and bottom of the conduction bands) beyond the ordinary DFT. Otherwise missing effects due to modification of the effective potential by SOC-induced spin-currents are quantified. Moreover, we carefully analyze the SOC-induced structural relaxation at the SCDFT level and determine its impact on the electronic structure of single-layer WSe_2.

All calculations are performed with a developer's version of the CRYSTAL package for electronic structure calculations of materials.[42,55] Reciprocal space of the 2D system is sampled on a regular 32 × 32 Monkhorst−Pack net within the reciprocal primitive cell, which corresponds to 61 and 1024 independent **k** points when symmetry is (without SOC) and is not (with SOC) exploited, respectively. Convergence of the self-consistent field (SCF) process is achieved when the difference in energy between two successive cycles does not exceed 1×10^{-9} a.u. Crystalline orbitals are expressed as linear

https://doi.org/10.1021/acs.jpclett.4c01607
J. Phys. Chem. Lett. 2024, 15, 7442−7448

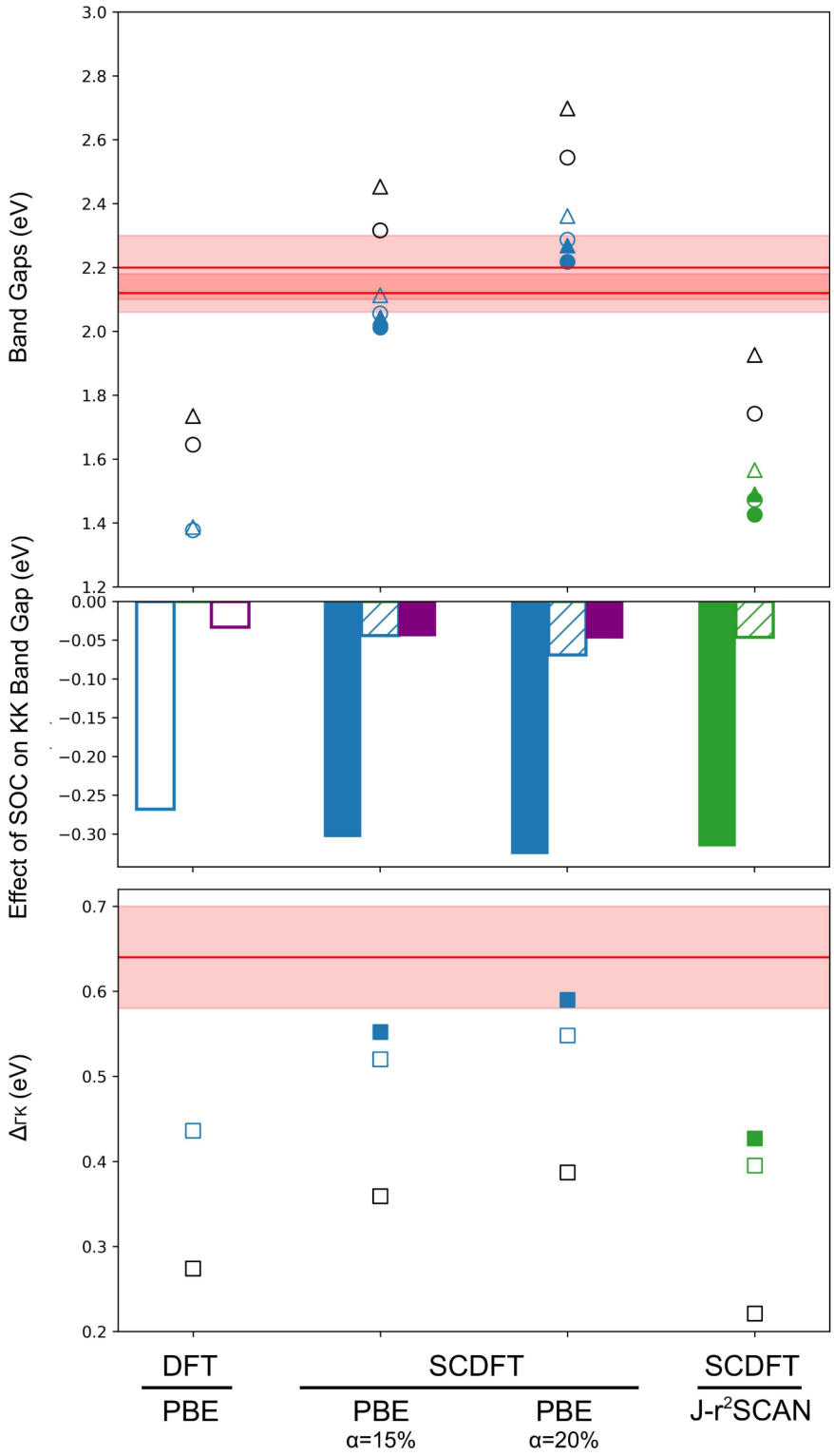

Figure 2. (Top panel) Direct Δ_{KK} (circles) and indirect Δ_{KQ} (triangles) band gap of single-layer WSe_2 from DFT and SCDFT calculations. Black symbols represent scalar-relativistic values (without SOC). Colored symbols are for calculations with SOC. Empty and full symbols correspond to calculations without and with a dependence on the spin current density $\vec{\mathbf{J}}$ of the xc potential, respectively. The horizontal red lines and areas mark the experimental values of 2.20 ± 0.10 eV and 2.12 ± 0.06 eV for the optical gap.[26] (Middle panel) Effect of SOC on the direct Δ_{KK} band gap. The first bar represents the total effect of SOC; the second bar, the effect of the inclusion of the spin current density $\vec{\mathbf{J}}$ on the xc potential; the third bar, the effect of SOC on the band gap due to its induced structural relaxation. (Bottom panel) Same as in the top panel for $\Delta_{\Gamma K}$. The horizontal red line and area mark the experimental value of 0.64 ± 0.06 eV.[26]

combinations of atomic orbitals.[56] We use the ECP60MDF and ECP28MDF effective-core potentials by Dolg and coworkers, for W and Se, respectively, derived from multiconfigurational four-component Dirac−Coulomb−Breit calculations.[57,58] The valence basis sets are those from ref 59. We use the PBE generalized-gradient approximation, GGA, xc

https://doi.org/10.1021/acs.jpclett.4c01607
J. Phys. Chem. Lett. 2024, 15, 7442−7448

functional (plain and hybridized with a fraction α of exact Fock exchange),[60] as well as the r^{2}SCAN meta-generalized-gradient, meta-GGA, xc functional,[61−63] in its original (SU(2) gauge-dependent) version and in its (SU(2) gauge-invariant), current-dependent version J-r^{2}SCAN.[53] SOC integrals are computed analytically for both the energy[64] and forces,[65] and SOC is treated self-consistently.[52,54,59,66−71]

The electronic band structure of single-layer WSe_2 is shown in Figure 1A, as computed with (blue line) and without (black line) SOC. The most important features of the band structure, including band gaps and band splittings, are highlighted. Figure 1A,D also shows the atomic structure of the system from side and top views, respectively. Based on experimental evidence, the system is likely to exhibit two nearly degenerate band gaps: a direct band gap at K, Δ_{KK}, and an indirect one Δ_{KQ}, with Q close to the midpoint along the $\Gamma-K$ path. Scanning tunneling spectroscopy measurements resulted in $\Delta_{KK} = 2.20 \pm 0.10$ eV and $\Delta_{KQ} = 2.12 \pm 0.06$ eV.[26] The direct and indirect band gap values obtained from our calculations are reported in Figure 2 (top panel), where they are compared to experimental values (red horizontal lines). Let us note that the calculated values are representative of fundamental band gaps, while the experimental values were obtained from optical experiments. Scalar relativistic values (obtained without SOC) are given as black symbols. Colored symbols are for calculations with SOC. Empty and full symbols correspond to calculations without and with a dependence on the spin current density $\vec{\mathbf{J}}$ of the xc potential, respectively. The effect of SOC on direct band gap Δ_{KK} is further highlighted in the middle panel of Figure 2. The following are observed: (i) In the absence of SOC, our calculations systematically describe $\Delta_{KK} < \Delta_{KQ}$ (i.e., a lower direct than indirect gap, with differences in the range of 0.12−0.20 eV). (ii) The inclusion of SOC systematically decreases both indirect and direct gaps, with a larger effect on the former, which brings the two transitions Δ_{KK} and Δ_{KQ} to be nearly degenerate (differences of 0.01 eV for PBE; 0.03 and 0.05 eV for hybrid PBE with fractions α of exact exchange of 15 and 20%, respectively; and 0.05 eV for J-r^{2}SCAN). (iii) The PBE and r^{2}SCAN xc functionals of the GGA and meta-GGA, respectively, tend to significantly underestimate the band gaps relative to the experimental values (i.e., by about 0.6 eV, that is by about 30%). As expected, the hybridization of PBE with a fraction α of exact exchange produces an increase in the computed band gaps. Optimal values of 2.0−2.3 eV are obtained with $\alpha = 0.15-0.20$. (iv) The effect of SOC on the direct gap from calculations with DFAs without $\vec{\mathbf{J}}$ is consistently around 0.26 eV (i.e., from PBE, hybrid PBE and r^{2}SCAN DFT calculations). (v) The inclusion of the SOC-induced spin current density $\vec{\mathbf{J}}$ on the xc functional within the SCDFT yields an extra effect on the gap of about 0.05−0.08 eV (i.e., about 20% of the total SOC effect).

The energy difference between the top of the VB at K and the top of the VB at Γ (see Figure 1 A for definition) has been measured by scanning tunneling spectroscopy: $\Delta_{\Gamma K} = 0.64 \pm 0.06$ eV.[26] Our computed values are compared to this experiment in the bottom panel of Figure 2. Scalar relativistic DFT calculations tend to systematically underestimate this value. SOC significantly affects this feature of the band structure, increasing it by about 0.15 eV with DFT and 0.2 eV with SCDFT. Thus, the inclusion of the spin current density $\vec{\mathbf{J}}$ on the xc functional is found to enhance the effect of SOC by an extra 25% in this case. In terms of absolute values, we observe that hybrid PBE gets close to the observed experimental value with just a slight underestimation (with α in the optimal range of 0.15−0.20 determined above from the analysis of band gaps). Interestingly, although J-r^{2}SCAN provides a significantly lower absolute value (due to a lower scalar relativistic value), it is found to quantitatively match the effect of SOC from hybrid PBE.

Let us now analyze SOC-induced Rashba band splittings in the single-layer WSe_2. The system exhibits a giant Rashba, type-I, splitting, Δ_v, at the top of the valence band (VB) at K (see Figure 1A for a graphical representation); a value of 513 ± 10 meV has been measured via angle-resolved photoemission spectroscopy (ARPES).[30] Many theoretical studies have tried to reproduce such a feature by use of different flavors of the DFT: a very consistent picture emerges with a systematic underestimation of the splitting by about 10−15%.[9,30,73−75] Here, we show that the inclusion of the spin current density $\vec{\mathbf{J}}$ on the many-body potential (i.e., the extension of DFT to SCDFT) precisely accounts for about 18% of the SOC-induced VB splitting in single-layer WSe_2, closing the gap between the computed splitting and the experimental value. We present our results in Figure 1B. The following are observed: (i) All calculations without spin currents in the xc potential (empty symbols) provide values of Δ_v in the range 410−425 meV, that is about 18% lower than the experimental value. (ii) The DFT values of 410−425 meV are consistent across different classes of xc functionals (pure GGA, hybrid GGA, and meta-GGA). (iii) The inclusion of the spin currents in the xc potential (i.e., SCDFT, full symbols) results in an increased value of Δ_v by about 18−20% either when currents are included explicitly (as in the J-r^{2}SCAN approach) or implicitly (as in the hybrid PBE approach, for optimal values of α of 0.15−0.20).

A SOC-induced Rashba band splitting, Δ_c, also occurs at the bottom of the conduction band (CB), as recently measured to 12 ± 0.5 meV at K by photoluminescence.[32] See Figure 1A for a graphical representation. Previous DFT investigations based on local density and generalized-gradient approximations (LDA and GGA) have systematically resulted in its overestimation with values of 38−40 meV.[73,75,76] We analyze such Rashba splitting in the conduction band along the whole $\Gamma-K$ path in Figure 1E, as computed without (dashed lines) and with (solid lines) inclusion of the spin current density in the xc potential. Results are presented for both strategies to SCDFT: explicit and implicit inclusion of $\vec{\mathbf{J}}$ in J-r^{2}SCAN (green lines) and hybrid PBE (blue lines), respectively. The following are observed: (i) The maximum Rashba splitting occurs at the Q point, with values as large as 300 meV. (ii) The effect of the inclusion of $\vec{\mathbf{J}}$ on the splitting close to Q is of about 70 meV (i.e., about 23% of the total). (iii) The computed value of Δ_c at K is about 15−20 meV, close to the experimental value of 12 ± 0.5 meV.

In conclusion, we stress that the key to these SCDFT results is the possibility to account for SOC self-consistently while employing energy functionals and effective potentials that depend (implicitly or explicitly) on spin currents. Indeed, it is this dependence on $\vec{\mathbf{J}}$ that unlocks a full SOC-induced orbital relaxation.[52,59] Without spin currents in the xc potential, any SOC-including calculation with a (semi)local DFA reduces to a second-variational post-self-consistent approach,[45] for all practical purposes. Figure 1C further shows this by comparing, on the same scale, the spin current $\mathbf{J}^z$ in the xy plane close to a Se atom computed without (top) and with (bottom) inclusion of $\vec{\mathbf{J}}$ in the xc potential. These orbital-relaxation effects on an

https://doi.org/10.1021/acs.jpclett.4c01607
J. Phys. Chem. Lett. 2024, 15, 7442−7448

SOC-induced quantity such as a spin current density are only possible within an SCDFT framework and can not be accounted for within the commonly used DFT framework.

We have shown that our two present strategies for SCDFT (explicit or implicit inclusion of $\vec{J}$ in J-r^{2}SCAN and hybrid GGA) both allow for an effective description of the effect of SOC on the electronic band structure. Crucially, SCDFT allows full capture of the giant Rashba band splitting in single-layer WSe_2, which is otherwise systematically underestimated by standard (semi)local DFAs within the DFT framework. We conclude by highlighting advantages and disadvantages of the two SCDFT$_{\vec{J}}$ approaches adopted here. J-r^{2}SCAN explicitly depends on $\vec{J}$ without adjustable parameters but leads to the underestimation of the band gaps. The hybrid functional approach, on the other hand, has an adjustable parameter α, but its optimization leads to an optimal description of band gaps and SOC-induced features of the band structure. Work is currently underway to develop further strategies for SCDFT, which may combine the advantages of both approaches.

AUTHOR INFORMATION

Corresponding Authors

Jacques K. Desmarais − *Dipartimento di Chimica, Università di Torino, 10125 Torino, Italy;* orcid.org/0000-0001-9199-1898; Email: jacqueskontak.desmarais@unito.it

Alessandro Erba − *Dipartimento di Chimica, Università di Torino, 10125 Torino, Italy;* orcid.org/0000-0002-2986-4254; Email: alessandro.erba@unito.it

Authors

Alberto Boccuni − *Dipartimento di Chimica, Università di Torino, 10125 Torino, Italy;* orcid.org/0000-0003-2613-7833

Bárbara Maria Teixeira Costa Peluzo − *Computational and Theoretical Chemistry Group (CATCO), Department of Chemistry, Southern Methodist University, Dallas, Texas 75275-0314, United States*

Filippo Bodo − *Computational and Theoretical Chemistry Group (CATCO), Department of Chemistry, Southern Methodist University, Dallas, Texas 75275-0314, United States*

Giacomo Ambrogio − *Dipartimento di Chimica, Università di Torino, 10125 Torino, Italy;* orcid.org/0009-0001-1194-3042

Jefferson Maul − *Dipartimento di Chimica, Università di Torino, 10125 Torino, Italy;* orcid.org/0000-0002-4920-1001

Davide Mitoli − *Dipartimento di Chimica, Università di Torino, 10125 Torino, Italy;* orcid.org/0000-0003-3940-2392

Giovanni Vignale − *Institute for Functional Intelligent Materials, National University of Singapore, Singapore 117544*

Stefano Pittalis − *Istituto Nanoscienze, Consiglio Nazionale delle Ricerche, I-41125 Modena, Italy*

Elfi Kraka − *Computational and Theoretical Chemistry Group (CATCO), Department of Chemistry, Southern Methodist University, Dallas, Texas 75275-0314, United States;* orcid.org/0000-0002-9658-5626

Complete contact information is available at: https://pubs.acs.org/10.1021/acs.jpclett.4c01607

Notes

The authors declare no competing financial interest.

ACKNOWLEDGMENTS

This research has received funding from the Project CH4.0 under the MUR program "Dipartimenti di Eccellenza 2023-2027" (CUP: D13C22003520001).

REFERENCES

(1) Chhowalla, M.; Shin, H. S.; Eda, G.; Li, L.-J.; Loh, K. P.; Zhang, H. The chemistry of two-dimensional layered transition metal dichalcogenide nanosheets. *Nat. Chem.* **2013**, *5*, 263−275.

(2) Kashid, R. V.; Late, D. J.; Chou, S. S.; Huang, Y.-K.; De, M.; Joag, D. S.; More, M. A.; Dravid, V. P. Enhanced field-emission behavior of layered MoS_2 sheets. *Small* **2013**, *9*, 2730−2734.

(3) Huang, X.; Zeng, Z.; Zhang, H. Metal dichalcogenide nanosheets: preparation, properties and applications. *Chem. Soc. Rev.* **2013**, *42*, 1934−1946.

(4) Cao, Y.; Mishchenko, A.; Yu, G.; Khestanova, E.; Rooney, A.; Prestat, E.; Kretinin, A.; Blake, P.; Shalom, M. B.; Woods, C.; et al. Quality heterostructures from two-dimensional crystals unstable in air by their assembly in inert atmosphere. *Nano Lett.* **2015**, *15*, 4914−4921.

(5) Mak, K. F.; Lee, C.; Hone, J.; Shan, J.; Heinz, T. F. Atomically thin MoS_2: a new direct-gap semiconductor. *Phys. Rev. Lett.* **2010**, *105*, 136805.

(6) Lee, C.; Yan, H.; Brus, L. E.; Heinz, T. F.; Hone, J.; Ryu, S. Anomalous lattice vibrations of single-and few-layer MoS_2. *ACS Nano* **2010**, *4*, 2695−2700.

(7) Molina-Sanchez, A.; Wirtz, L. Phonons in single-layer and few-layer MoS_2 and WS_2. *Phys. Rev. B* **2011**, *84*, 155413.

(8) Eda, G.; Yamaguchi, H.; Voiry, D.; Fujita, T.; Chen, M.; Chhowalla, M. Photoluminescence from chemically exfoliated MoS_2. *Nano Lett.* **2011**, *11*, 5111−5116.

(9) Kang, J.; Tongay, S.; Zhou, J.; Li, J.; Wu, J. Band offsets and heterostructures of two-dimensional semiconductors. *Appl. Phys. Lett.* **2013**, *102*, No. 012111.

(10) Sahin, H.; Tongay, S.; Horzum, S.; Fan, W.; Zhou, J.; Li, J.; Wu, J.; Peeters, F. Anomalous Raman spectra and thickness-dependent electronic properties of WSe_2. *Phys. Rev. B* **2013**, *87*, 165409.

(11) Ataca, C.; Sahin, H.; Ciraci, S. Stable, single-layer MX_2 transition-metal oxides and dichalcogenides in a honeycomb-like structure. *J. Phys. Chem. C* **2012**, *116*, 8983−8999.

(12) Pu, J.; Yomogida, Y.; Liu, K.-K.; Li, L.-J.; Iwasa, Y.; Takenobu, T. Highly flexible MoS_2 thin-film transistors with ion gel dielectrics. *Nano Lett.* **2012**, *12*, 4013−4017.

(13) Eda, G.; Maier, S. A. Two-dimensional crystals: managing light for optoelectronics. *ACS Nano* **2013**, *7*, 5660−5665.

(14) Akinwande, D.; Petrone, N.; Hone, J. Two-dimensional flexible nanoelectronics. *Nat. Commun.* **2014**, *5*, 5678.

(15) Huang, J.-K.; Pu, J.; Hsu, C.-L.; Chiu, M.-H.; Juang, Z.-Y.; Chang, Y.-H.; Chang, W.-H.; Iwasa, Y.; Takenobu, T.; Li, L.-J. Large-area synthesis of highly crystalline WSe_2 monolayers and device applications. *ACS Nano* **2014**, *8*, 923−930.

(16) Daus, A.; Vaziri, S.; Chen, V.; Köroğlu, Ç.; Grady, R. W.; Bailey, C. S.; Lee, H. R.; Schauble, K.; Brenner, K.; Pop, E. High-performance flexible nanoscale transistors based on transition metal dichalcogenides. *Nat. Electron.* **2021**, *4*, 495−501.

(17) Kuc, A.; Zibouche, N.; Heine, T. Influence of quantum confinement on the electronic structure of the transition metal sulfide TS_2. *Phys. Rev. B* **2011**, *83*, 245213.

(18) Kumar, A.; Ahluwalia, P. Electronic structure of transition metal dichalcogenides monolayers 1H-MX 2 (M= Mo, W; X= S, Se, Te) from ab-initio theory: new direct band gap semiconductors. *Eur. Phys. J. B* **2012**, *85*, 186.

(19) Radisavljevic, B.; Radenovic, A.; Brivio, J.; Giacometti, V.; Kis, A. Single-layer MoS_2 transistors. *Nat. Nanotechnol.* **2011**, *6*, 147−150.

(20) Fang, H.; Chuang, S.; Chang, T. C.; Takei, K.; Takahashi, T.; Javey, A. High-performance single layered WSe_2 p-FETs with chemically doped contacts. *Nano Lett.* **2012**, *12*, 3788−3792.
(21) Tongay, S.; Zhou, J.; Ataca, C.; Lo, K.; Matthews, T. S.; Li, J.; Grossman, J. C.; Wu, J. Thermally driven crossover from indirect toward direct bandgap in 2D semiconductors: $MoSe_2$ versus MoS_2. *Nano Lett.* **2012**, *12*, 5576−5580.
(22) Wang, L.; Kutana, A.; Yakobson, B. I. Many-body and spin-orbit effects on direct-indirect band gap transition of strained monolayer MoS_2 and WS_2. *Ann. Phys.* **2014**, *526*, L7−L12.
(23) Lezama, I. G.; Arora, A.; Ubaldini, A.; Barreteau, C.; Giannini, E.; Potemski, M.; Morpurgo, A. F. Indirect-to-direct band gap crossover in few-layer $MoTe_2$. *Nano Lett.* **2015**, *15*, 2336−2342.
(24) Steinhoff, A.; Kim, J.-H.; Jahnke, F.; Rosner, M.; Kim, D.-S.; Lee, C.; Han, G. H.; Jeong, M. S.; Wehling, T.; Gies, C. Efficient excitonic photoluminescence in direct and indirect band gap monolayer MoS_2. *Nano Lett.* **2015**, *15*, 6841−6847.
(25) Wang, Y.; Cong, C.; Yang, W.; Shang, J.; Peimyoo, N.; Chen, Y.; Kang, J.; Wang, J.; Huang, W.; Yu, T. Strain-induced direct−indirect bandgap transition and phonon modulation in monolayer WS_2. *Nano Res.* **2015**, *8*, 2562−2572.
(26) Zhang, C.; Chen, Y.; Johnson, A.; Li, M.-Y.; Li, L.-J.; Mende, P. C.; Feenstra, R. M.; Shih, C.-K. Probing critical point energies of transition metal dichalcogenides: surprising indirect gap of single layer WSe_2. *Nano Lett.* **2015**, *15*, 6494−6500.
(27) Hsu, W.-T.; Lu, L.-S.; Wang, D.; Huang, J.-K.; Li, M.-Y.; Chang, T.-R.; Chou, Y.-C.; Juang, Z.-Y.; Jeng, H.-T.; Li, L.-J.; et al. Evidence of indirect gap in monolayer WSe_2. *Nat. Commun.* **2017**, *8*, 929.
(28) Blundo, E.; Felici, M.; Yildirim, T.; Pettinari, G.; Tedeschi, D.; Miriametro, A.; Liu, B.; Ma, W.; Lu, Y.; Polimeni, A. Evidence of the direct-to-indirect band gap transition in strained two-dimensional WS_2, MoS_2, and WSe_2. *Phys. Rev. Res.* **2020**, *2*, No. 012024.
(29) Zhu, Z. Y.; Cheng, Y. C.; Schwingenschlögl, U. Giant spin-orbit-induced spin splitting in two-dimensional transition-metal dichalcogenide semiconductors. *Phys. Rev. B* **2011**, *84*, 153402.
(30) Le, D.; Barinov, A.; Preciado, E.; Isarraraz, M.; Tanabe, I.; Komesu, T.; Troha, C.; Bartels, L.; Rahman, T. S.; Dowben, P. A. Spin−orbit coupling in the band structure of monolayer WSe_2. *J. Phys.: Condens. Matter* **2015**, *27*, 182201.
(31) Song, Y.; Dery, H. Transport Theory of Monolayer Transition-Metal Dichalcogenides through Symmetry. *Phys. Rev. Lett.* **2013**, *111*, No. 026601.
(32) Ren, L.; Robert, C.; Dery, H.; He, M.; Li, P.; Van Tuan, D.; Renucci, P.; Lagarde, D.; Taniguchi, T.; Watanabe, K.; et al. Measurement of the conduction band spin-orbit splitting in WSe_2 and WS_2 monolayers. *Phys. Rev. B* **2023**, *107*, 245407.
(33) Zibouche, N.; Kuc, A.; Musfeldt, J.; Heine, T. Transition-metal dichalcogenides for spintronic applications. *Ann. Phys.* **2014**, *526*, 395−401.
(34) Kuc, A.; Heine, T. The electronic structure calculations of two-dimensional transition-metal dichalcogenides in the presence of external electric and magnetic fields. *Chem. Soc. Rev.* **2015**, *44*, 2603−2614.
(35) Cheng, Y.; Zhu, Z.; Tahir, M.; Schwingenschlögl, U. Spin-orbit−induced spin splittings in polar transition metal dichalcogenide monolayers. *EPL* **2013**, *102*, 57001.
(36) Li, W.-F.; Fang, C.; van Huis, M. A. Strong spin-orbit splitting and magnetism of point defect states in monolayer WS_2. *Phys. Rev. B* **2016**, *94*, 195425.
(37) Roldan, R.; López-Sancho, M. P.; Guinea, F.; Cappelluti, E.; Silva-Guillén, J. A.; Ordejón, P. Momentum dependence of spin−orbit interaction effects in single-layer and multi-layer transition metal dichalcogenides. *2D Mater.* **2014**, *1*, No. 034003.
(38) Kormányos, A.; Zólyomi, V.; Drummond, N. D.; Rakyta, P.; Burkard, G.; Fal'Ko, V. I. Monolayer MoS_2: Trigonal warping, the Γvalley, and spin-orbit coupling effects. *Phys. Rev. B* **2013**, *88*, No. 045416.
(39) Kormányos, A.; Zólyomi, V.; Drummond, N. D.; Burkard, G. Spin-orbit coupling, quantum dots, and qubits in monolayer transition metal dichalcogenides. *Phys. Rev. X* **2014**, *4*, No. 011034.
(40) Giannozzi, P.; Andreussi, O.; Brumme, T.; Bunau, O.; Nardelli, M. B.; Calandra, M.; Car, R.; Cavazzoni, C.; Ceresoli, D.; Cococcioni, M.; et al. Advanced capabilities for materials modelling with Quantum ESPRESSO. *J. Phys.: Condens. Matter* **2017**, *29*, 465901.
(41) Hafner, J. Ab-initio simulations of materials using VASP: Density-functional theory and beyond. *J. Comput. Chem.* **2008**, *29*, 2044−2078.
(42) Erba, A.; Desmarais, J. K.; Casassa, S.; Civalleri, B.; Doná, L.; Bush, I. J.; Searle, B.; Maschio, L.; Edith-Daga, L.; Cossard, A.; et al. CRYSTAL23: A Program for Computational Solid State Physics and Chemistry. *J. Chem. Theory Comput.h* **2023**, *19*, 6891−6932.
(43) Díaz-Sánchez, L.; Romero, A.; Cardona, M.; Kremer, R.; Gonze, X. Effect of the spin-orbit interaction on the thermodynamic properties of crystals: Specific heat of bismuth. *Phys. Rev. Lett.* **2007**, *99*, 165504.
(44) Fernández-Seivane, L.; Oliveira, M. A.; Sanvito, S.; Ferrer, J. On-site approximation for spin−orbit coupling in linear combination of atomic orbitals density functional methods. *J. Phys.: Condens. Matter* **2006**, *18*, 7999.
(45) Huhn, W. P.; Blum, V. One-hundred-three compound band-structure benchmark of post-self-consistent spin-orbit coupling treatments in density functional theory. *Phys. Rev. Mater.* **2017**, *1*, No. 033803.
(46) Bencheikh, K. SpinÄiorbit coupling in the spin-current-density-functional theory. *J. Phys. A* **2003**, *36*, 11929.
(47) Vignale, G.; Rasolt, M. Current- and spin-density-functional theory for inhomogeneous electronic systems in strong magnetic fields. *Phys. Rev. B* **1988**, *37*, 10685−10696.
(48) Tokatly, I. V. Equilibrium Spin Currents: Non-Abelian Gauge Invariance and Color Diamagnetism in Condensed Matter. *Phys. Rev. Lett.* **2008**, *101*, 106601.
(49) Droghetti, A.; Rungger, I.; Rubio, A.; Tokatly, I. V. Spin-orbit induced equilibrium spin currents in materials. *Phys. Rev. B* **2022**, *105*, No. 024409.
(50) Pittalis, S.; Vignale, G.; Eich, F. G. $U(1) \times SU(2)$gauge invariance made simple for density functional approximations. *Phys. Rev. B* **2017**, *96*, No. 035141.
(51) Abedinpour, S. H.; Vignale, G.; Tokatly, I. Gauge-invariant formulation of spin-current density-functional theory. *Phys. Rev. B* **2010**, *81*, 125123.
(52) Desmarais, J. K.; Ambrogio, G.; Vignale, G.; Erba, A.; Pittalis, S. Generalized Kohn-Sham approach for the electronic band structure of spin-orbit coupled materials. *Phys. Rev. Mater.* **2024**, *8*, No. 013802.
(53) Desmarais, J. K.; Maul, J.; Civalleri, B.; Erba, A.; Vignale, G.; Pittalis, S. Spin Currents via the Gauge Principle for Meta-Generalized Gradient Exchange-Correlation Functionals. *Phys. Rev. Lett.* **2024**, *132*, 256401.
(54) Bodo, F.; Desmarais, J. K.; Erba, A. Spin current density functional theory of Weyl semimetals. *Phys. Rev. B* **2022**, *105*, 125108.
(55) Erba, A.; Baima, J.; Bush, I.; Orlando, R.; Dovesi, R. Large Scale Condensed Matter DFT Simulations: Performance and Capabilities of the Crystal Code. *J. Chem. Theory Comput.* **2017**, *13*, 5019−5027.
(56) Desmarais, J.; Erba, A.; Dovesi, R. Generalization of the Periodic LCAO Approach in the CRYSTAL Code to *g*-type Orbitals. *Theor. Chem. Acc.* **2018**, *137*, 28.
(57) Figgen, D.; Peterson, K. A.; Dolg, M.; Stoll, H. Energy-consistent pseudopotentials and correlation consistent basis sets for the 5d elements Hf−Pt. *J. Chem. Phys.* **2009**, *130*, 164108.
(58) Stoll, H.; Metz, B.; Dolg, M. Relativistic energy-consistent pseudopotentialsÂiRecent developments. *J. Comput. Chem.* **2002**, *23*, 767−778.
(59) Desmarais, J. K.; Boccuni, A.; Flament, J.-P.; Kirtman, B.; Erba, A. Perturbation Theory Treatment of Spin−Orbit Coupling. III: Coupled Perturbed Method for Solids. *J. Chem. Theory Comput.h* **2023**, *19*, 1853−1863.

https://doi.org/10.1021/acs.jpclett.4c01607
J. Phys. Chem. Lett. 2024, 15, 7442−7448

(60) Perdew, J. P.; Burke, K.; Ernzerhof, M. *Phys. Rev. Lett.* **1996**, *77*, 3865.
(61) Furness, J. W.; Kaplan, A. D.; Ning, J.; Perdew, J. P.; Sun, J. Accurate and numerically efficient r2SCAN meta-generalized gradient approximation. *J. Phys. Chem. Lett.* **2020**, *11*, 8208−8215.
(62) Bartók, A. P.; Yates, J. R. Regularized SCAN functional. *J. Chem. Phys.* **2019**, *150*, 161101.
(63) Sun, J.; Ruzsinszky, A.; Perdew, J. P. Strongly constrained and appropriately normed semilocal density functional. *Phys. Rev. Lett.* **2015**, *115*, No. 036402.
(64) Desmarais, J. K.; Flament, J.-P.; Erba, A. Spin-orbit coupling from a two-component self-consistent approach. I. Generalized Hartree-Fock theory. *J. Chem. Phys.* **2019**, *151*, No. 074107.
(65) Desmarais, J. K.; Erba, A.; Flament, J.-P. Structural relaxation of materials with spin-orbit coupling: Analytical forces in spin-current DFT. *Phys. Rev. B* **2023**, *108*, 134108.
(66) Desmarais, J. K.; Flament, J.-P.; Erba, A. Spin-orbit coupling in periodic systems with broken time-reversal symmetry: Formal and computational aspects. *Phys. Rev. B* **2020**, *101*, 235142.
(67) Desmarais, J. K.; Komorovsky, S.; Flament, J.-P.; Erba, A. Spin−orbit coupling from a two-component self-consistent approach. II. Non-collinear density functional theories. *J. Chem. Phys.* **2021**, *154*, 204110.
(68) Desmarais, J. K.; Flament, J.-P.; Erba, A. Fundamental role of fock exchange in relativistic density functional theory. *J. Phys. Chem. Lett.* **2019**, *10*, 3580−3585.
(69) Desmarais, J. K.; Flament, J.-P.; Erba, A. Adiabatic connection in spin-current density functional theory. *Phys. Rev. B* **2020**, *102*, 235118.
(70) Desmarais, J. K.; Erba, A.; Flament, J.-P.; Kirtman, B. Perturbation Theory Treatment of Spin−Orbit Coupling II: A Coupled Perturbed Kohn−Sham Method. *J. Chem. Theory Comput.h* **2021**, *17*, 4712−4732.
(71) Comaskey, W. P.; Bodo, F.; Erba, A.; Mendoza-Cortes, J. L.; Desmarais, J. K. Role of spin currents on electron-electron interaction in the quantum spin Hall phase. *Phys. Rev. B* **2022**, *106*, No. L201109.
(72) Camino, B.; Zhou, H.; Ascrizzi, E.; Boccuni, A.; Bodo, F.; Cossard, A.; Mitoli, D.; Ferrari, A. M.; Erba, A.; Harrison, N. M. CRYSTALpytools: a Python Infrastructure for the CRYSTAL Code. *Comput. Phys. Commun.* **2023**, *292*, 108853.
(73) Kośmider, K.; González, J. W.; Fernández-Rossier, J. Large spin splitting in the conduction band of transition metal dichalcogenide monolayers. *Phys. Rev. B* **2013**, *88*, 245436.
(74) Zhu, Z.; Cheng, Y.; Schwingenschlögl, U. Giant spin-orbit-induced spin splitting in two-dimensional transition-metal dichalcogenide semiconductors. *Phys. Rev. B* **2011**, *84*, 153402.
(75) Kormányos, A.; Burkard, G.; Gmitra, M.; Fabian, J.; Zólyomi, V.; Drummond, N. D.; FalÄôko, V. k· p theory for two-dimensional transition metal dichalcogenide semiconductors. *2D Mater.* **2015**, *2*, No. 022001.
(76) Echeverry, J.; Urbaszek, B.; Amand, T.; Marie, X.; Gerber, I. C. Splitting between bright and dark excitons in transition metal dichalcogenide monolayers. *Phys. Rev. B* **2016**, *93*, 121107.

https://doi.org/10.1021/acs.jpclett.4c01607
J. Phys. Chem. Lett. 2024, 15, 7442−7448